





Unraveling intricate properties of exchange-coupled bilayers by means of broadband ferromagnetic resonance and spin pumping experiments

M. Arana ^{1,2}, M. Gamino ^{2,3}, A. B. Oliveira,³ J. Holanda ^{2,*}, A. Azevedo ²,
S. M. Rezende,² and R. L. Rodríguez-Suárez^{4,5}

¹*Instituto de Física, Universidade Federal do Rio de Janeiro, 21941-909 Rio de Janeiro, Rio de Janeiro, Brazil*

²*Departamento de Física, Universidade Federal de Pernambuco, 50670-901 Recife, Pernambuco, Brazil*

³*Departamento de Física, Universidade Federal do Rio Grande do Norte, 59078-900 Natal, Rio Grande do Norte, Brazil*

⁴*Facultad de Física, Pontificia Universidad Católica de Chile, Avenida Vicuña Mackenna 4860, Casilla 306, Santiago, Chile*

⁵*Centro de Investigación en Nanotecnología y Materiales Avanzados CIEN-UC, Pontificia Universidad Católica de Chile, Avenida Vicuña Mackenna 4860, Casilla 306, Santiago, Chile*



(Received 4 May 2020; revised 13 July 2020; accepted 28 July 2020; published 3 September 2020)

Ferromagnetic resonance (FMR) measurements using a broadband microstrip excitation technique were performed at room temperature for an antiferromagnetic/ferromagnetic (AF/FM) bilayer of $\text{Ir}_{20}\text{Mn}_{80}(35.0\text{ nm})/\text{Ni}_{81}\text{Fe}_{19}(7.5\text{ nm})$. The angular dependence of the resonance field was measured for several excitation frequencies ranging from 1.5 to 10.0 GHz. From the numerical fitting of the experimental data, it was observed that the exchange bias field (H_E) and the rotatable anisotropy field (H_{RA}) originating from the exchange interaction at the AF/FM interface are frequency dependent. The results were explained considering the coexistence of ferromagnetic and antiferromagnetic coupling at the AF/FM interface. We also investigated the spin pumping voltage generated in the structure of $\text{Ir}_{20}\text{Mn}_{80}(35.0\text{ nm})/\text{Ni}_{81}\text{Fe}_{19}(7.5\text{ nm})/\text{Pt}(4\text{ nm})$ and showed that from the voltage peaks occurring at the ferromagnetic resonance condition it is possible to reproduce the FMR dispersion relation.

DOI: [10.1103/PhysRevB.102.104405](https://doi.org/10.1103/PhysRevB.102.104405)

I. INTRODUCTION

Antiferromagnetic (AF) coupling with ferromagnets (FMs) is a source of intense research due mainly to several advances in applications [1–8]. In the last few years, discoveries of the spin Hall effect in metallic AFs [9–12] and spin transport in several AFs [13–17], have renewed the attention to AF/FM bilayers. One important phenomenon related to this coupling is the exchange bias (EB) effect. This effect in AF/FM materials has been a subject of study for no less than six decades [1–3,18,19].

The best-known manifestation of the EB effect in AF/FM bilayers is the unidirectional shift of the magnetic hysteresis curve along the field axis set by the magnetic field applied during the growth process (EB direction). Another two manifestations emerge in ferromagnetic resonance (FMR) measurements, namely (a) symmetry breaking of the usual FMR angular dependence, and (b) the isotropic shift of the resonance field in polycrystalline AF/FM bilayers, due to the rotatable anisotropy [20–23]. In order to explain these simultaneous observations, the models [20–25] consider the existence of two types of grains in polycrystalline AF layers, stable ones (or nonrotatable) and other unstable (or rotatable), both coupled to the adjacent FM magnetization. The former are responsible for the exchange anisotropy characterized by the exchange

bias field (H_E) and the latter by the isotropic shift of the resonance field characterized by a rotatable anisotropy field (H_{RA}).

In a previous work [23], we studied the rotatable and exchange anisotropies in AF/FM bilayers of $\text{Ir}_{20}\text{Mn}_{80}(t)/\text{Ni}_{81}\text{Fe}_{19}(7.5\text{ nm})$ for three samples with AF thickness of, $t = 5, 10,$ and 35 nm . A Brillouin light-scattering technique was used to measure the azimuthal angle dependence of the magnon frequency at fixed magnetic field values of 50, 200, and 1000 Oe from which the anisotropy fields H_{RA} and H_E were extracted. The results showed a nonmonotonic dependence of both fields with the external field value. In particular, the sample $\text{Ir}_{20}\text{Mn}_{80}(35.0\text{ nm})/\text{Ni}_{81}\text{Fe}_{19}(7.5\text{ nm})$, presented a negative value for H_{RA} at low-field strengths. These results were explained considering the coexistence of parallel and antiparallel coupling at the AF/FM interface.

In this paper, we report the investigation of the exchange and rotatable anisotropies in the $\text{Ir}_{20}\text{Mn}_{80}(35.0\text{ nm})/\text{Ni}_{81}\text{Fe}_{19}(7.5\text{ nm})$ bilayer through FMR experiments using a microstrip transmission line setup by varying the azimuthal angle between the external magnetic field and the EB direction. In particular, we explore the low-frequency regime in which the resonance fields are on the order of the anisotropy fields. Using the rotatable and exchange anisotropies fields H_{RA} and H_E , strengths have a nonmonotonic dependence with the excitation frequency providing an additional tunable source of anisotropy. Additionally, through the spin pumping voltage generated in a structure of AF/FM/Pt, we explore the spin to charge current conversion by injecting a spin current from the biased FM film, via the spin pumping effect, into

*Present address: Departamento de Física, Universidade Federal do Espírito Santo, 29060-900 Vitória, Espírito Santo, Brazil.

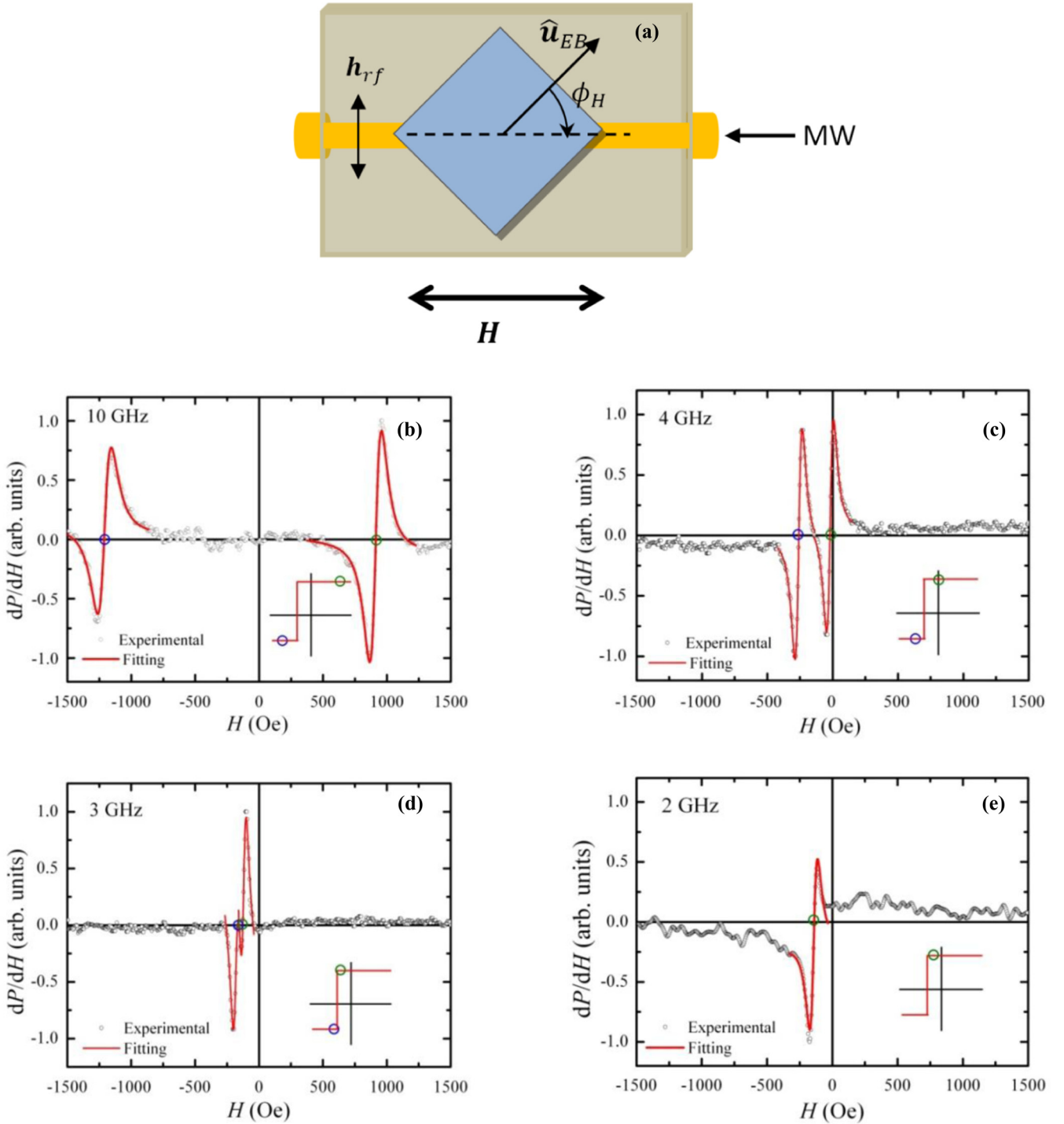


FIG. 1. (a) Sketch of the broadband FMR setup used for FMR absorption measurements in the AF/FM bilayer of IrMn(35 nm)/Py. (b) Derivative of the FMR absorption spectrum of IrMn(35 nm)/Py for the DC field, parallel ($\phi_H = 0^\circ$) and antiparallel ($\phi_H = 180^\circ$) to the FM uniaxial axis, with excitation frequencies of (b) 10 GHz, (c) 4 GHz, (d) 3.0 GHz, and (e) 2.0 GHz.

the Pt thin film, which made it possible to reproduce the experimental FMR measurements.

II. EXPERIMENT

The AF/FM bilayer of Si(001)/Ni₈₁Fe₁₉(3)/Ir₂₀Mn₈₀(35)/Ni₈₁Fe₁₉(7.5) herein studied was prepared by the DC magnetron sputtering technique. In order to produce

a Ir₂₀Mn₈₀ (henceforth denoted by IrMn) film with antiferromagnetic order, and to fix the EB direction [\hat{u}_{EB} in Fig. 1(a)], prior to its deposition, a 3-nm-thick layer of Ni₈₁Fe₁₉ (permalloy, henceforth named Py) was grown on Si(001) substrate of $5.0 \times 2.5 \text{ mm}^2$ under an external applied static magnetic field of about 200 Oe [23]. To prevent spurious effects due to metal interdiffusion, no capping layer was deposited on top of the multilayer.

For the ferromagnetic resonance (FMR) and spin pumping (SP) voltage measurements we used a microwave signal provided by a generator with a tunable frequency in the range of 1.5 – 10.0 GHz with power up to 100 mW. The broadband FMR spectrometer consists of a rf frequency sweeper that feeds a microstrip line of copper, 0.5 mm wide with characteristic impedance around 50 Ω , fabricated on a Duroid substrate with a ground plane. The IrMn/Py sample is placed face down on the microstrip line, separated by a 60- μm -thick Mylar sheet and the transmitted rf radiation is detected by a Schottky diode. By sweeping the external DC field, applied perpendicular to the h_{rf} , at the ferromagnetic resonance an enhancement of rf-power absorption takes place, which is detected by Schottky diode. As the DC field varies the absorption power can be measured using two different methods: (i) by measuring the Lorentzian absorption curve directly by a nanovoltmeter, or (ii) by measuring the derivative of the Lorentzian absorption curve by means of the lock-in detection. In the latter method, the DC field is modulated by an external AC magnetic field of amplitude 0.2 Oe and frequency of 8.7 kHz generated by a pair of Helmholtz coils, thus generating the absorption derivative spectrum as the field is scanned, as shown in Figs. 1(b)–1(e). The FMR measurements were performed, for several values of the azimuthal angle ϕ_H , between the field and the EB direction of the sample (see Fig. 1) from 0 to 360° and for frequency values from 1.5 to 10.0 GHz, increasing the frequency in steps of 0.5 GHz. Starting from a saturated condition, the external magnetic field was varied in the range ± 1550.0 Oe, with a field step of 5.0 Oe, and dwelling time of 100 ms per step.

For the spin pumping (SP) experiments, a 4-nm-thick film of Pt with lateral dimensions of $1 \times 3 \text{ mm}^2$ was deposited by DC sputtering on the top of the IrMn/Py bilayer such that the final sample was Si/Py(3 nm)/IrMn(35 nm)/Py(7.5 nm)/Pt(4 nm). As illustrated in Fig. 4, two thin copper wires were attached to the extremes of the Pt line, 3.0 mm apart, with silver paint. The copper electrodes were directly connected to a nanovoltmeter for measuring the DC voltage generated by the inverse spin Hall effect (ISHE) in the Pt layer as the spin current is injected across the Py/Pt interface by the SP process.

III. MODEL

In order to improve the interpretation of the experimental data, we carried out calculations of the FMR dispersion relation, from dependence of the frequency on the applied magnetic field in the AF/FM bilayer. The calculation is based on the magnetic free-energy procedure, established by Smith and Beljers [26] and Suhl [27], that was later adapted for

exchange-bias bilayers [22,23,28,29]:

$$\left(\frac{\omega}{\gamma}\right)^2 = \frac{1}{(t_{\text{FM}}M_{\text{FM}})^2} \times \left[\left(\mathcal{E}_{\phi_{\text{FM}}\phi_{\text{FM}}} - \frac{\mathcal{E}_{\phi_{\text{FM}}\phi_{\text{AF}}}^2}{\mathcal{E}_{\phi_{\text{AF}}\phi_{\text{AF}}}} \right) \left(\mathcal{E}_{\theta_{\text{FM}}\theta_{\text{FM}}} - \frac{\mathcal{E}_{\theta_{\text{FM}}\theta_{\text{AF}}}^2}{\mathcal{E}_{\theta_{\text{AF}}\theta_{\text{AF}}}} \right) \right], \quad (1)$$

where, γ is the gyromagnetic ratio and t_{FM} and M_{FM} are the FM layer thickness and saturation magnetization, respectively. The terms \mathcal{E}_{ij} denote the second derivative of the free energy per unit area with respect to the equilibrium angles of the FM magnetization and the corresponding AF sublattice magnetization in contact with the AF layer.

The phenomenological model for the free energy per unit area, necessary to obtain the ω vs H dependence through Eq. (1), considers the relevant interactions of the FM/AF system,

$$\mathcal{E} = (-\mathbf{H} \cdot \mathbf{M}_{\text{FM}})t_{\text{FM}} + \mathcal{E}_{u,d}^{\text{FM}} + \mathcal{E}_E^{\text{AF/FM}} + \mathcal{E}_{\text{RA}}^{\text{AF}}. \quad (2)$$

In Eq. (2), the first term is the Zeeman energy, the second term, $\mathcal{E}_{u,d}^{\text{FM}}$, groups the uniaxial and demagnetizing contributions to the free energy of the FM layer, and the third, $\mathcal{E}_E^{\text{AF/FM}}$, and fourth, $\mathcal{E}_{\text{RA}}^{\text{AF}}$, terms consider the exchange coupling at the AF/FM interface and the contribution of the unstable anti-ferromagnetic grains through the rotatable anisotropy, respectively. As the last two terms in Eq. (2) are the most relevant for the subsequent discussion, we write them explicitly as

$$\mathcal{E}_{\text{RA}}^{\text{AF}} = -K_{ra} \left(\frac{\mathbf{M}_{\text{FM}} \cdot \hat{\mathbf{h}}}{M_{\text{FM}}} \right)^2, \quad (3)$$

and

$$\mathcal{E}_E^{\text{AF/FM}} = -J_E \frac{\mathbf{M}_{\text{FM}} \cdot \mathbf{M}_{\text{AF}}}{M_{\text{FM}}M_{\text{AF}}} - \sigma_W \frac{\mathbf{M}_{\text{FM}} \cdot \hat{\mathbf{u}}_{\text{EB}}}{M_{\text{AF}}}, \quad (4)$$

where K_{ra} is the rotatable anisotropy constant, J_E is the interfacial exchange coupling constant (taken as positive for ferromagnetic coupling), and σ_W ($\sim \sqrt{K_{\text{AF}}}$) is the energy per unit surface of a 90° domain wall at the AF side of the interface, K_{AF} being its anisotropy constant. The unit vectors $\hat{\mathbf{u}}_{\text{EB}}$ and $\hat{\mathbf{h}} = \mathbf{H}/H$ represent the EB direction and the applied magnetic field direction, respectively. Here we consider that the FM uniaxial anisotropy axis is parallel to the EB direction. Details of the anisotropies involved in the second term $\mathcal{E}_{u,d}^{\text{FM}}$ can be found elsewhere [22–25].

Considering that the FM magnetization is saturated for the values of the magnetic fields at which the FMR occurs, the relation between the resonance field H_R as function of the azimuthal angles of \mathbf{H} (ϕ_H) and \mathbf{M}_{FM} (ϕ_{FM}) obtained from Eqs. (1)–(4) can be written as

$$H_R = \frac{1}{2 \cos(\phi_H - \phi_{\text{FM}})} \left[H_U(1 - 3\cos^2\phi_{\text{FM}}) - 4\pi M_{\text{eff}} - 2H_{\text{RA}} - H_1^{(\phi_{\text{FM}}, \phi_{\text{AF}})} - H_2^{(\phi_{\text{FM}}, \phi_{\text{AF}})} + \sqrt{[H_U \sin^2\phi_H + 4\pi M_{\text{eff}} + H_1(\phi_{\text{FM}}, \phi_{\text{AF}}) - H_2(\phi_{\text{FM}}, \phi_{\text{AF}})]^2 + 4\left(\frac{\omega}{\gamma}\right)^2} \right], \quad (5)$$

where

$$H_1^{(\phi_{\text{FM}}, \phi_{\text{AF}})} = \frac{H_W \cos \phi_{\text{AF}} \cos(\phi_{\text{FM}} - \phi_{\text{AF}} - \beta) - H_E \sin^2(\phi_{\text{FM}} - \phi_{\text{AF}} - \beta)}{\frac{H_W}{H_E} \cos \phi_{\text{AF}} + \cos(\phi_{\text{FM}} - \phi_{\text{AF}} - \beta)} \quad (6)$$

and

$$H_2^{(\phi_{\text{FM}}, \phi_{\text{AF}})} = \frac{H_W \cos \phi_{\text{AF}} \cos(\phi_{\text{FM}} - \phi_{\text{AF}} - \beta)}{\frac{H_W}{H_E} \cos \phi_{\text{AF}} + \cos(\phi_{\text{FM}} - \phi_{\text{AF}} - \beta)}. \quad (7)$$

Here, $H_U (= 2K_u/M_{\text{FM}})$ is the FM uniaxial anisotropy field, $H_E [= J_E/(t_{\text{FM}}M_{\text{FM}})]$ is the effective exchange-coupling field at the FM/AF interface, $H_{\text{RA}} (= 2K_{\text{ra}}/M_{\text{FM}})$ is the effective rotatable anisotropy field, $H_W [= \sigma_W/(t_{\text{FM}}M_{\text{FM}})]$ is the effective domain-wall field, and M_{eff} is the effective magnetization. The angle β is introduced in the model to account for the misalignment between the AF and FM easy axes [20].

IV. RESULTS AND DISCUSSION

The full FMR absorption spectrum of the IrMn/Py bilayer was measured varying the applied field strength in the setup sketched in Fig. 1(a); each value of the in-plane resonance field H_R was determined by fitting the derivative of the Lorentzian line shape of the measured spectra shown in Figs. 1(b)–1(e). The experiment was repeated for different frequencies ranging from 1.5 to 10.0 GHz, allowing the determination of the experimental dispersion relation shown in Fig. 2 for the external magnetic field H applied at $\phi_H = 0^\circ$ (positive values) and $\phi_H = 180^\circ$ (negative values).

To understand the conditions at which FMR occurs we consider \mathbf{M}_{AF} parallel to the $\hat{\mathbf{u}}_{\text{EB}}$ direction, which is supported by the condition $H_W \gg H_E$, as observed in our sample [22,23]. In this case, $\phi_{\text{AF}} \cong 0$ and when the field is applied along the

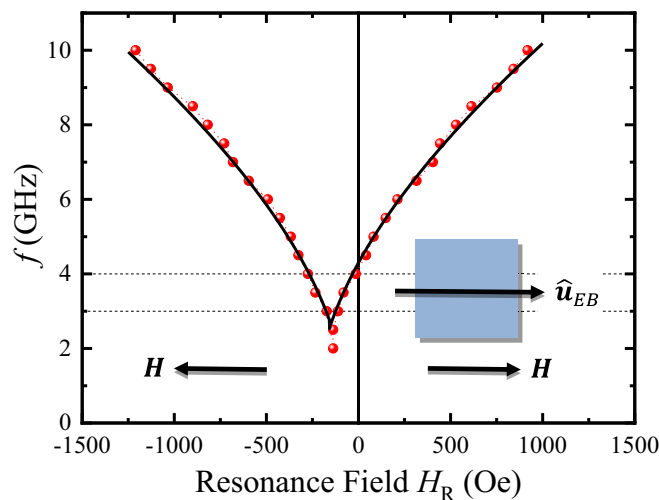


FIG. 2. Experimental dispersion relation of the IrMn(35 nm)/Py(7.5 nm) bilayers (red symbols). The external magnetic field is applied along the easy axis. The solid line is a numerical fit using for $H_E = 150$ Oe, $H_{\text{RA}} = 80$ Oe, and $H_U = 15$ Oe. The values of H_E and H_{RA} correspond to the mean values for $3 \text{ GHz} \leq f \leq 4 \text{ GHz}$ in Fig. 3.

easy axis, the resonance field from Eq. (5), can be written as

$$H_R \approx \frac{1}{2 \cos(\phi_H - \phi_{\text{FM}})} [\mathcal{B}(\omega) - 2H_E \cos \phi_{\text{FM}}], \quad (8)$$

where $\mathcal{B}(\omega) = -2H_U - 4\pi M_{\text{eff}} - 2H_{\text{RA}} + \sqrt{(4\pi M_{\text{eff}})^2 + 4(\frac{\omega}{\gamma})^2}$. When the excitation frequency is greater than 4 GHz (see Fig. 2), $\mathcal{B}(\omega) > 2H_E$ and the resonant fields occur for $\phi_{\text{FM}} = \phi_H$ at $\phi_H = 0^\circ$ for $|H_{R1}| = [\mathcal{B}(\omega) - 2H_E]/2$ (left branch in Fig. 2) and $\phi_H = 180^\circ$ for $|H_{R2}| = [\mathcal{B}(\omega) + 2H_E]/2$ (right branch in Fig. 2). The difference between $|H_{R1}|$ and $|H_{R2}|$ values, with $|H_{R1}| < |H_{R2}|$, is due to the fact that in the former case, when the magnetization is oriented along the energy minimum (parallel to $\hat{\mathbf{u}}_{\text{EB}}$), FMR occurs at a lower field compared with the last case in which it is oriented along the hard axis direction (antiparallel to $\hat{\mathbf{u}}_{\text{EB}}$). This is also what is observed in Fig. 1(b), with two resonant fields at $H_{R1} = 912.0$ Oe ($\phi_{\text{FM}} = \phi_H = 0^\circ$) and $H_{R2} = -1209.0$ Oe ($\phi_{\text{FM}} = \phi_H = 180^\circ$).

For excitation frequencies, $3 \text{ GHz} \leq f \leq 4 \text{ GHz}$, as shown in Figs. 1(d) and 1(e), $\mathcal{B}(\omega) < 2H_E$, and we still have two resonant fields, one at a lower value for $\phi_{\text{FM}} = 0$ and $\phi_H = 180^\circ$ (H_{R1}) and the other for $\phi_{\text{FM}} = \phi_H = 180^\circ$ (H_{R2}). Note that at H_{R1} , although $\phi_H = 180^\circ$, due to the EB field the FM magnetization is parallel to EB direction [see inset in Fig. 1(d) (green circle)]. Measurements at frequencies lower than 3 GHz as shown in Fig. 2, and Fig. 1(e) for 2 GHz, reveal that there is only one resonant field value. In this case, $\mathcal{B}(\omega) + 2H_E < 0$ and the FMR can only occur at one field value for $\phi_H = 180^\circ$ and $\phi_{\text{FM}} = 0^\circ$ maintained at this direction by the EB field. No resonant fields will be observed for frequency values lower than 1.5 GHz. The solid line in Fig. 2 represents the dispersion relation calculated from Eq. (5) for the mean values of the anisotropy fields ($H_E = 155$ Oe, $H_{\text{RA}} = 103$ Oe) between 3 and 10.0 GHz.

The FMR absorption measurements were repeated varying the azimuthal angle from 0 to 360° for every fixed excitation frequency. Figure 3(a) shows the in-plane angular dependence of the resonance field for the sample IrMn(35.0 nm)/Py measured at different frequencies. Experimental values denoted by the symbols correspond to the H_{R1} values shown by the green circles in Figs. 1(b)–1(e). For H_{R2} , we obtained similar values but shifted by 180° . The solid lines are fits using Eq. (5). For the numerical calculations, the effective magnetization value $4\pi M_{\text{eff}} = 9.38$ kG and uniaxial anisotropy field $H_U = 15$ Oe were extracted from the fit of the FMR experimental data corresponding to the unbiased Py(7.5 nm)/Si thin film (see Refs. [20,21]) with a gyromagnetic ratio of $\gamma = 17.6$ GHz/kOe. Figure 3(b) shows the rotatable H_{RA} and exchange H_E anisotropy fields as a function of the excitation frequency. The error bars were obtained from two measurements at each azimuthal angle and dashed lines are guides to the eyes. As we can observe, both fields are almost constant

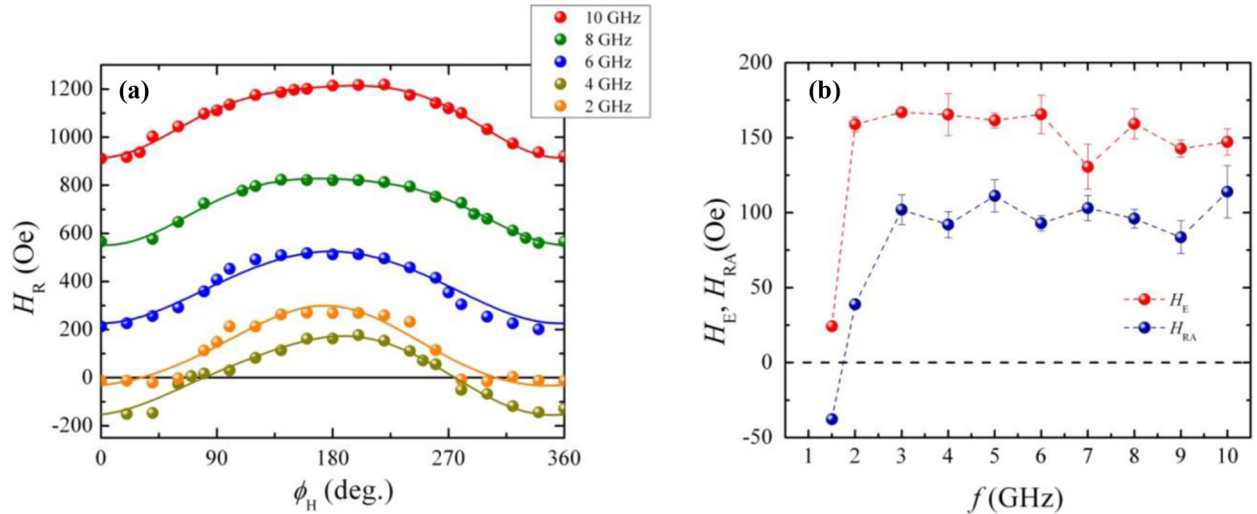


FIG. 3. (a) In-plane angular dependence of the resonance fields of the IrMn(35 nm)/Py bilayer for selected frequencies of 10, 8, 6, 4, and 2 GHz. The continuous lines are the fittings of the experimental data using Eq. (5). (b) Exchange bias field (H_E) and rotatable anisotropy field (H_{RA}) strengths obtained from the best fittings of the FMR data. The dashed lines are guides to the eyes.

with f for frequencies higher than 3 GHz and drastically diminish in the low-frequency regime.

These experimental observations are in agreement with the Brillouin light-scattering measurements reported in our previous work on the same sample [23] where we considered the coexistence of parallel and antiparallel coupling at the AF/FM interface, which also agrees with other investigations on the same system [25,30–32]. Essentially, we considered the presence of AF grains at the AF/FM interface that could be ferromagnetically (FMC) or antiferromagnetically (AFC) coupled to the FM magnetization. Each type of grain classified as unstable (either superparamagnetic or rotatable) or stable (pinned) differs in number and in anisotropy energy, being able to rotate their magnetization at different field strengths. Thereby, the lower the grain anisotropy energy, the smaller the field required to rotate its magnetization.

In the FMR experiment, the excitation frequency is fixed and the resonance field varies as a function of the azimuthal angle ϕ_H resulting in bell-shaped curves, as shown in Fig. 3(a). As the magnetic field regime, at which resonance occurs, is proportional to the excitation frequency, the behavior of the FMC and AFC grains will depend on it. While pinned, the magnetization of both grains contributes only to EB, which can be positive (for FMC) or negative (for AFC). On the other hand, for unpinned grains their magnetization loses the pinning condition, thus not contributing to H_E , and start to be responsible for H_{RA} . The trend shown in Fig. 3(b) can be explained considering that in our sample of IrMn(35.0 nm)/Py, FMC grains exceed AFC ones in number and in anisotropy energy what is supported by the concave bell shape of the FMR field [23]. For $f = 1.5$ GHz the rotatable anisotropy field H_{RA} obtained from the numerical fitting is negative. This is explained considering that at low-field values (low frequency) those AFC grains having lower anisotropy rotate contributing to a negative value of H_{RA} [23]. At the same time, those with higher anisotropy energies are pinned in the $-\hat{u}_{EB}$ direction and in competition with the pinned

FMC ones (pinned \parallel to $+\hat{u}_{EB}$), thus diminishing H_E . When the field further increases, an increasing number of FMC grains (much higher than AFC ones) begin to rotate their magnetization, thus contributing to a positive value of H_{RA} . In the same sense, the magnetization of AFC grains that are now rotating does not compete with the pinned FMC ones and H_E saturates.

Once the dynamical response of the magnetization has been studied, we measured the spin pumping voltage in the IrMn(35 nm)/Py(7.5 nm)/Pt structure. Spin pumping voltages (V_{SPE}) generated in hybrid structures result from a combination of two effects, the SP effect, in which the precessing magnetization in FMR condition injects a spin current into an adjacent layer, and the inverse spin Hall effect (ISHE), that converts the injected spin current into a transverse charge current of density $\mathbf{J}_C = \theta_{SH}(2e/\hbar)\mathbf{J}_S \times \boldsymbol{\sigma}$, \mathbf{J}_S being the spin current density (in units of angular momentum/area · time), θ_{SH} is the spin Hall angle, and $\boldsymbol{\sigma}$ is the spin polarization. In the experimental setup, the spin current flows perpendicularly to the plane producing a voltage V_{SPE} that we measured at the ends of a 3×1 -mm² Pt line, 4 nm thick, deposited on the top of the IrMn(35 nm)/Py(7.5 nm) in the setup shown in Fig. 4(a).

Driving the FMR strip line with a microwave of fixed frequency and varying the external magnetic field \mathbf{H} we can measure the peaks of V_{ISHE} occurring at the FMR condition, as expected from the dispersion relation. Note that, as the propagation direction of the spin current is fixed, the sign of the V_{SPE} peaks is given by the polarization direction $\boldsymbol{\sigma}$. This means that, according to Fig. 4(a), as the spin Hall angle θ_{SH} is positive for Pt [22], the measured V_{SPE} peak will be positive when the magnetization is in the EB direction and negative in the other case. This observation permits us to know the magnetization direction in the FM layer.

These experiments were repeated for several frequencies and the results were consistent with the dispersion relation obtained by FMR, as shown in Fig. 5. Similar results were

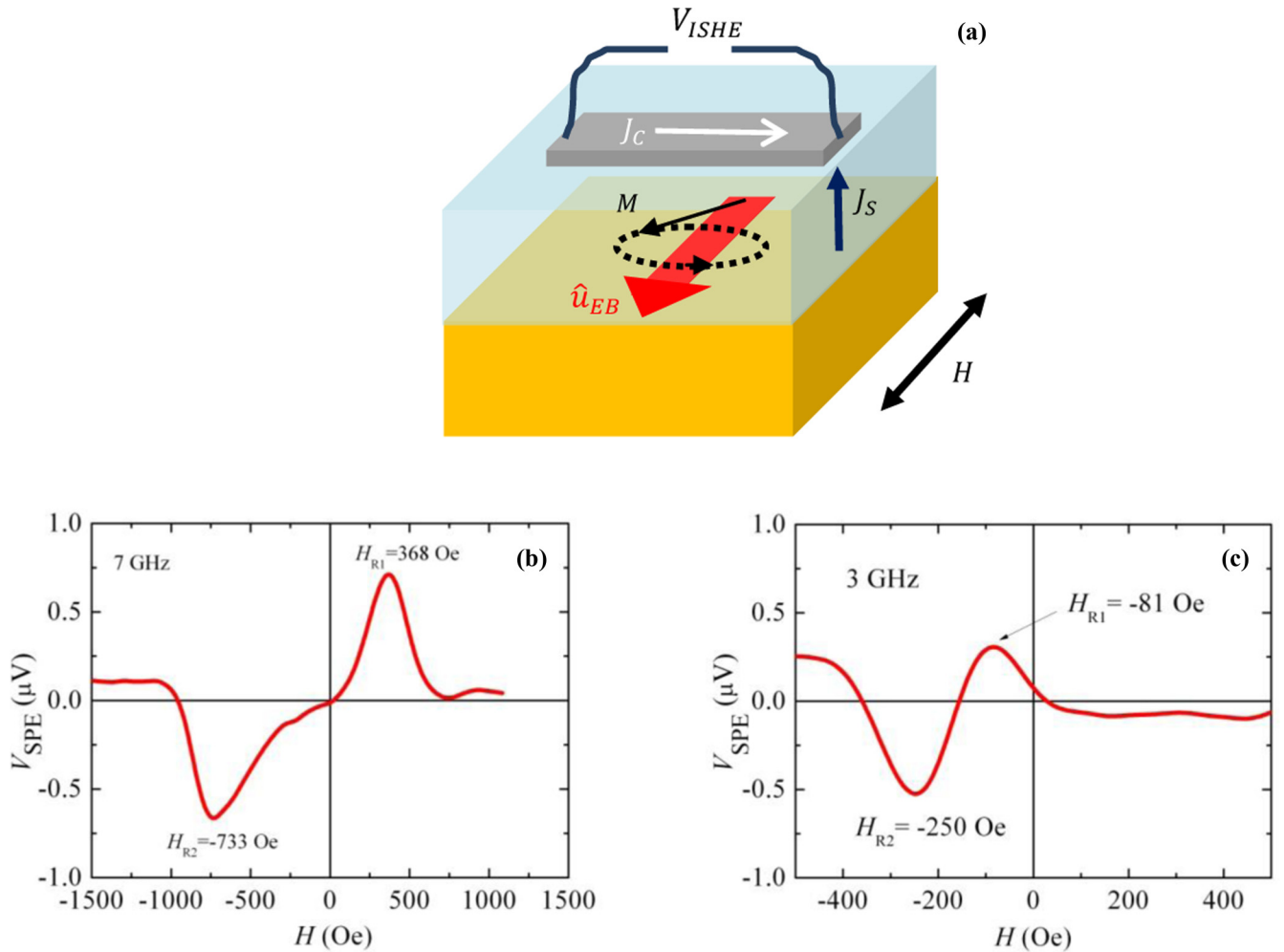


FIG. 4. (a) Sketch showing the IrMn/Py bilayer and the Pt line on the top of the Py layer used to measure the DC voltage due to the ISHE charge current resulting from the spin current produced by microwave FMR spin pumping at (b) 7 GHz and (c) 3 GHz.

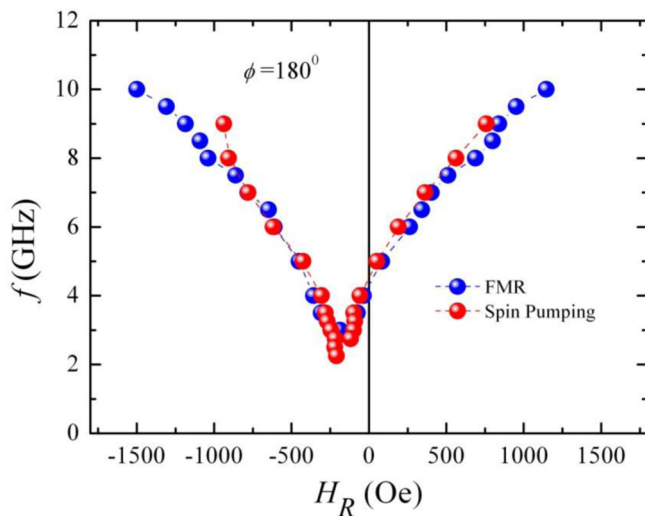


FIG. 5. Full dispersion relation of the Py(7.5 nm)/IrMn(35 nm) bilayer determined by FMR (red dots) and spin pumping experiments (blue dots) in the antiparallel configuration. The dashed lines are guides for the eyes.

observed when the sample is rotated by 180° but with a shift to the right because of the exchange field.

V. CONCLUSIONS

In this work we used broadband ferromagnetic resonance to measure the resonance field as a function of the in-plane angle for different excitation frequencies, in a bilayer of IrMn(35 nm)/Py(7.5 nm). The experimental results were interpreted using a model that considers the principal contributions to the magnetic energy of the system and the coexistence of stable and unstable AF grains with ferromagnetic and antiferromagnetic coupling at the interface. We show that in concordance with the model both the exchange bias and rotatable anisotropy fields are strongly dependent on the frequency values in the low regime of excitation frequencies. This could provide an additional source to tune the magnetic anisotropies in hybrids exchange biased bilayers. We also reproduced the dispersion relation through the spin pumping voltages showing that this kind of experiment could be effective to study the spin to charge conversion in AF/FM bilayers. This could also be useful to explore the spin transport through AF materials.

ACKNOWLEDGMENTS

This research was supported in Brazil by Conselho Nacional de Desenvolvimento Científico e Tecnológico (CNPq), Coordenação de Aperfeiçoamento de Pessoal de Nível Super-

rior (CAPES), Financiadora de Estudos e Projetos (FINEP), and Fundação de Amparo a Ciência e Tecnologia do Estado de Pernambuco (FACEPE), and in Chile by Fondo Nacional de Desarrollo Científico y Tecnológico (FONDECYT), Grant No. 1170723.

-
- [1] W. H. Meiklejohn and C. P. Bean, *Phys. Rev.* **102**, 1413 (1956).
- [2] A. E. Berkowitz and K. Takano, *J. Magn. Magn. Mater.* **200**, 552, (1999).
- [3] J. Nogués and I. K. Schuller, *J. Magn. Magn. Mater.* **192**, 203 (1999).
- [4] W. Zhang and K. M. Krishnan, *Mater. Sci. Eng., R* **105**, 1 (2016).
- [5] M. B. Jungfleisch, W. Zhang, and A. Hoffmann, *Phys. Lett. A* **382**, 865 (2018).
- [6] J. R. Fermin, M. A. Lucena, A. Azevedo, F. M. de Aguiar, and S. M. Rezende, *J. Appl. Phys.* **87**, 6421 (2000).
- [7] S. S. P. Parkin, K. P. Roche, M. G. Samant, P. M. Rice, R. B. Beyers, R. E. Scheuerlein, E. J. O'Sullivan, S. L. Brown, J. Bucchigano, D. W. Abraham, Y. Lu, M. Rooks, P. L. Trouilloud, R. A. Wanner, and W. J. Gallagher, *J. Appl. Phys.* **85**, 5828 (1999).
- [8] S. A. Wolf, D. D. Awschalom, R. A. Buhrman, J. M. Daughton, S. von Molnár, M. L. Roukes, A. Y. Chtchelkanova, and D. M. Treger, *Science* **294**, 1488 (2001).
- [9] H. Chen, Q. Niu, and A. H. MacDonald, *Phys. Rev. Lett.* **112**, 017205 (2014).
- [10] J. B. S. Mendes, R. O. Cunha, O. Alves Santos, P. R. T. Ribeiro, F. L. A. Machado, R. L. Rodríguez-Suárez, A. Azevedo, and S. M. Rezende, *Phys. Rev. B* **89**, 140406(R) (2014).
- [11] W. Zhang, M. B. Jungfleisch, W. Jiang, J. E. Pearson, A. Hoffmann, F. Freimuth, and Y. Mokrousov, *Phys. Rev. Lett.* **113**, 196602 (2014).
- [12] J. Holanda, H. Saglam, V. Karakas, Z. Zang, Y. Li, R. Divan, Y. Liu, O. Ozatay, V. Novosad, J. E. Pearson, and A. Hoffmann, *Phys. Rev. Lett.* **124**, 087204 (2020).
- [13] P. Merodio, A. Ghosh, C. Lemonias, E. Gautier, U. Ebels, M. Chshiev, H. Béa, V. Baltz, and W. E. Bailey, *Appl. Phys. Lett.* **104**, 032406 (2014).
- [14] H. Wang, C. Du, P. C. Hammel, and F. Yang, *Phys. Rev. B* **91**, 220410(R) (2015).
- [15] W. Lin, K. Chen, S. Zhang, and C. L. Chien, *Phys. Rev. Lett.* **116**, 186601 (2016).
- [16] M. Arana, M. Gamino, E.F. Silva, V. M. T. S. Barthem, D. Givord, A. Azevedo, and S. M. Rezende, *Phys. Rev. B* **98**, 144431 (2018).
- [17] J. Holanda, D. S. Maior, A. Azevedo, and S. M. Rezende, *J. Magn. Magn. Mater.* **432**, 507 (2017).
- [18] S. Khanal, A. Diaconu, J. M. Vargas, D. R. Lenormand, C. Garcia, C. A. Ross, and L. Spinu, *J. Phys. D: Appl. Phys.* **47**, 255002 (2014).
- [19] J. B. Mohammadi, J. M. Jones, S. Paul, B. Khodadadi, C. K. A. Mewes, T. Mewes, and C. Kaiser, *Phys. Rev. B* **95**, 064414 (2017).
- [20] R. D. McMichael, M. D. Stiles, P. J. Chen, and W. F. Egelhoff, Jr., *Phys. Rev. B* **58**, 8605 (1998).
- [21] M. D. Stiles and R. D. McMichael, *Phys. Rev. B* **59**, 3722 (1999).
- [22] R. L. Rodríguez-Suárez, L. H. Vilela-Leão, T. Bueno, A. B. Oliveira, J. R. L. de Almeida, P. Landeros, S. M. Rezende, and A. Azevedo, *Phys. Rev. B* **83**, 224418 (2011).
- [23] R. L. Rodríguez-Suárez, A. B. Oliveira, F. Estrada, D. S. Maior, M. Arana, O. Alves Santos, A. Azevedo, and S. M. Rezende, *J. Appl. Phys.* **123**, 043901 (2018).
- [24] J. Geshev, L. G. Pereira, and J. E. Schmidt, *Phys. Rev. B* **66**, 134432 (2002).
- [25] S. Nicolodi, L. G. Pereira, A. Harres, G. M. Azevedo, J. E. Schmidt, I. García-Aguilar, N. M. Souza-Neto, C. Deranlot, F. Petroff, and J. Geshev, *Phys. Rev. B* **85**, 224438 (2012).
- [26] J. Smit and H. G. Beljers, *Philips Res. Rep.* **10**, 113 (1955).
- [27] H. Suhl, *Phys. Rev.* **97**, 555 (1955).
- [28] J. Geshev, L. G. Pereira, and J. E. Schmidt, *Phys. Rev. B* **64**, 184411 (2001).
- [29] R. L. Rodríguez-Suárez, S. M. Rezende, and A. Azevedo, *Phys. Rev. B* **71**, 224406 (2005).
- [30] S. K. Mishra, F. Radu, H. A. Dürr, and W. Eberhardt, *Phys. Rev. Lett.* **102**, 177208 (2009).
- [31] D. Schafer, P. L. Grande, L. G. Pereira, G. M. Azevedo, A. Harres, M. A. de Sousa, P. Pelegrini, and J. Geshev, *J. Appl. Phys.* **117**, 215301 (2015).
- [32] G. Salazar-Alvarez, J. J. Kavich, J. Sort, A. Muarza, S. Stepanow, A. Potenza, H. Marchetto, S. S. Dhesi, V. Naltz, B. Dieny, A. Weber, L. J. Heyderman, J. Nogués, and P. Gambardella, *Appl. Phys. Lett.* **95**, 012510 (2009).